Available online at www.sciencedirect.com

SciVerse ScienceDirect

Ceramics International 39 (2013) 1443–1449

CERAMICS INTERNATIONAL

www.elsevier.com/locate/ceramint

Preparation and characterization of lotus ceramics with different pore sizes and their implication for the generation of microbubbles for CO_2 sequestration applications

Catalin Popa[a,*], Ken-ichi Katsumata[b], Toshihiro Isobe[a], Nobuhiro Matsushita[b], Akira Nakajima[a], Taisuke Kurata[c], Kiyoshi Okada[a,b]

[a]*Department of Metallurgy and Ceramics Science, Tokyo Institute of Technology, S7-708, O-okayama, Meguro, Tokyo 152-8552, Japan*
[b]*Materials and Structures Laboratory, Tokyo Institute of Technology, R3-507, Nagatsuta, Midori, Yokohama, Kanagawa 226-8502, Japan*
[c]*Kurata Refractory Inc., Hirono, Futaba, Fukushima 979-0402, Japan*

Received 15 June 2012; received in revised form 26 July 2012; accepted 26 July 2012
Available online 5 August 2012

Abstract

Four kinds of porous mullite ceramics, named lotus ceramics because of the similarity of their microstructure with lotus roots, were prepared by an extrusion method using rayon fibers of four different diameters (8.1, 9.6, 16.8 and 37.6 μm) as the pore formers. The physicochemical properties of these samples were characterized to test their applicability for the generation of microbubbles. The lotus ceramic samples contained pores of 9.4, 10, 15.6 and 30 μm size and porosities of 45–48%. SEM micrographs confirmed that the cylindrical pores were oriented unidirectionally along the extrusion direction and the degree of alignment was greater with larger fiber diameter. The permeability for gaseous CO_2 increased with increasing pore size from 3×10^{-13} to 8×10^{-13} m^2. The four lotus ceramic samples, a commercial air stone (72 μm) and two simple tubes (1000 and 3500 μm) were used to generate microbubbles in water under ambient conditions from a gas mixture of CO_2 and air. It was found that the bubble size could be decreased with bubblers of smaller pore size. In the bubble size measurements for pure CO_2 and air, the air bubbles were larger than the CO_2 bubbles due to partial dissolution of CO_2 into the water during bubbling. In order to generate smaller size bubbles using porous ceramic bubblers, the liquid must penetrate through the pores of the lotus ceramics before the gas is introduced into the system.

Keywords: A. Extrusion; B. Fibers; B. Microstructure-final; D. Mullite

1. Introduction

Porous ceramics have attracted much interest due to their high porosity, permeability and chemical durability under harsh usage conditions [1]. Well-controlled microstructures of pore size and pore distribution permit various applications of porous ceramics, including filtration, purification, catalysis, sorption, etc [1]. These porous ceramics can be categorized in terms of their porous microstructures as: 3D-type with three-dimensionally connected and distributed open pores, 2D-type with slit-shaped open pores and 1D-type with unidirectionally oriented pores [2]. Porous ceramics with 1D-type microstructures have advantages of high permeability [3] and capillary lift [4] due to their unique porous microstructure. Various techniques have been reported for the preparation of 1D-type porous ceramics, including oriented solidification, templating, anodic oxidation, extrusion, etc [2]. Extrusion is widely used in industry due to its ease of fabrication of large products. The extrusion can be achieved either by a multi-pass method [5] or by using flammable fibers as the pore formers [3]. The former method has an advantage of being able to tune the pore size by changing the repeated extrusion conditions, but has the disadvantage of being a lengthy process. This latter disadvantage of the multi-pass method can be overcome by using flammable fibers as pore formers, enabling single-pass extrusion to be used. The resulting porous

*Corresponding author. Tel.: +81 45 924 5323; fax: +81 45 924 5338.
E-mail address: popa.c.aa@m.titech.ac.jp (C. Popa).

0272-8842/$ - see front matter © 2012 Elsevier Ltd and Techna Group S.r.l. All rights reserved.
http://dx.doi.org/10.1016/j.ceramint.2012.07.087

ceramics are called lotus ceramics due to the similarity of their microstructure with lotus roots [4].

An advantage of lotus ceramics is their high permeability arising from the controlled porous microstructure. We therefore believe that lotus ceramics are suitable for the generation of small mists and bubbles through their well-controlled porous microstructure. Small bubbles are reported to be effective in ensuring a high gas dissolution rate. Decreasing the pore size of the lotus ceramics is expected to decrease the bubble size. Small bubbles can lead to a higher specific surface area, longer retention time in the liquid phase and higher internal pressure. Recently the generation of microbubbles has attracted much attention. The research in this area focuses mainly on devices to generate micrometer size bubbles, i.e. microfluidic devices that mix the aqueous phase with gaseous CO_2 [6], Shirasu porous glass [7], micro-pore plates [8], rotational porous plates [9] and submerged orifices using ultrasound waves [10].

We have developed lotus ceramics containing unidirectionally aligned through-pores by an extrusion method using flammable fibers with various diameters. These show excellent gas permeability (for both CO_2 and N_2) as well as good mechanical strength due to the well-controlled porous microstructures. The microstructures of these samples showed pore sizes in agreement with the diameters of the pore formers. The efficiency of lotus ceramics in generating small size bubbles even at low gas pressure has already been demonstrated [11]. Bubbles generated from pores and nozzles are generally called Fritz bubbles because their size can be evaluated using the Fritz equation [12], $r_B=(3\gamma r_P/(2\rho g))^{1/3}$, where r_B=is the bubble radius, γ is the surface tension, r_P is the pore radius, ρ is the density and g is gravitational acceleration. Since the pore size of the resulting lotus ceramics was about 16 μm, the bubble size calculated from the Fritz equation [12] was about 900 μm, very much different from the observed bubble size. The reason for such a distinct difference is not clear at present.

The aim of the present work was to prepare and characterize lotus ceramics with different pore sizes and to investigate the characteristics of bubble generation using these lotus ceramics, from the point of view of possible CO_2 sequestration applications.

2. Experimental section

The starting materials were alumina (Showa Denko, Japan), kaolin clay from Kentucky, USA (Morimura, Japan) and Chinese earthen clay (Inagaki Mining, Japan). The average particle size of these powders was 4.7, 1.0 and 20 μm, respectively. The Chinese clay was used to promote liquid-phase sintering and lower the firing temperature. The bulk composition of the mixtures was formulated to contain Al_2O_3 SiO_2 and Fe_2O_3 contents of 56, 36 and 5 mass%, corresponding to the principal crystalline phase mullite. The powder batches were dry mixed with 20 mass% rayon fibers (0.8T, 1.1T, 3.3T and 17TDtex Tow, Omikenshi, Japan) of average fiber diameter 8.1, 9.6, 16.8 and 37.6 μm, chopped to 800 μm lengths by Chubu Pile Ind., Japan. The mixtures were kneaded with 40 mass% water and molded using an extruder (Setogawa Industries, Japan). The dimensions of the extruder barrel and inner aperture were 95 and 50 mm, respectively. Tubular green bodies with inner and outer diameters of 20–50 mm were extruded using an outlet die. The extruded green bodies were dried at room temperature for 3 day, then at 120 °C for 18 h before being fired at 1500 °C for 2 h in air. The various lotus ceramics (LC) samples used in the present experiments are designated as LC followed by the value of their specific pore size (in μm). The LC samples with different pore sizes were prepared by using various rayon fiber diameters, e.g. 8.1 μm (LC9.4), 9.6 μm (LC10), 16.8 μm (LC15.6) and 37.6 μm (LC30). The dimensions (length, outer diameter and inner diameter) of each of the LC samples were 150 mm × 47 mm × 38 mm. For comparison we tested a commercial bubbler (CB72, Ibuki air stone, Ibuki, Japan) of dimensions 350 mm × 23 mm × 10 mm and pore size 72 μm, a micropipette tip (T1000) with an inner diameter of 1000 μm and a polymeric tube (T3500) with an inner diameter of 3500 μm. The bubbling pressures were 5, 7, 11, 18, 24, 38 and 38 kPa for the T3500, T1000, CB72, LC30, LC15.6, LC10 and LC9.4 bubblers, respectively.

The bulk densities and porosities of the four lotus ceramics were measured by the Archimedes technique using water. Their pore size distributions and pore volumes were measured by mercury intrusion porosimetry (Pascal 240, Carlo Elba, Italy) with a maximum injection pressure of about 200 MPa. The contact angle and surface tension used for the calculation was 130° and 0.485 N/m, respectively.

LC bubblers were prepared by plugging up both ends of the lotus ceramics using rubber stoppers. In all the experiments the gas was fed from a gas cylinder at a controlled gas pressure (0.2 MPa) and flow rate (0.5 L/min) through a polymeric gas tube inserted in one of the rubber stoppers. The flow rate was measured just before the gas entry point to the bubbler by a flow meter (Kofloc, Japan), and the pressure was determined by using a pressure gauge (Migishita Seiki, Japan). The gas was fed through a polymeric gas tube to the bubbler located in a transparent water container. In each experiment, 60 L of tap water was added to the container. Before the start of each experiment, the lotus ceramics were pre-cleaned in an ultrasonic bath to clear the pores of any impurities, then immersed in the water container for 30 min for the water to penetrate through LC pores, thus wetting the LC.

The temperature and pH were measured using a portable pH meter incorporating a thermometer (SevenGo, Metler-Toledo, Switzerland). The CO_2 concentration in tap water was recorded by a CO_2 detector (CGP-1, TOA-DKK, Japan). The resulting data were corrected for temperature and pH of the solution to adjust for the effect of carbonate ion [13]. The pictures of the bubble sizes were

recorded by a Casio Exilim EX-F1 high speed digital camera with 36–432 mm lens. A backlight lamp was used in order to obtain bright, clear shots of the bubbles. The pictures were analyzed by Image *J* 1.45 r software [14]. 1000–2000 bubbles were counted for the LC samples, but only 100–200 bubbles were counted for T1000, T3500 and CB72 due to the smaller number of bubbles generated. Thus, several hundred bubbles (up to 1500) were counted in the analyzed segment of each photograph. Since the minimum bubble size that could be analyzed by the present experiment was 60 μm, bubbles smaller than this size were neglected.

3. Results and discussion

3.1. Physicochemical characterization

The XRD pattern of the LC samples (Fig. 1) confirmed that the main constituent is mullite ($3Al_2O_3 \cdot 2SiO_2$). Other minor peaks might be due to Fe-based compounds formed by liquid phase sintering of the initial starting materials at high temperatures.

The pore size distributions of the four lotus ceramics LC9.4, LC10, LC15.6 and LC30 and CB72 are shown in Fig. 2. The results of the Hg-porosity measurements are in good agreement with the diameter of the pore formers shown in parentheses. The resulting pore sizes of LC9.4 and LC10 were slightly enlarged while those of LC15.6 and LC30 shrank during firing. The shrinkage of the pores is generally observed due to sintering but the reason for the enlargement of the pores in samples LC9.4 and LC10 is unclear at present.

A commercial bubbler CB72 was used for comparison with the LC samples. Its pore size (Fig. 2) was 72 μm and its crystalline phase (Fig. 1) was α-alumina with minor accessory phases of quartz, cristobalite and feldspar.

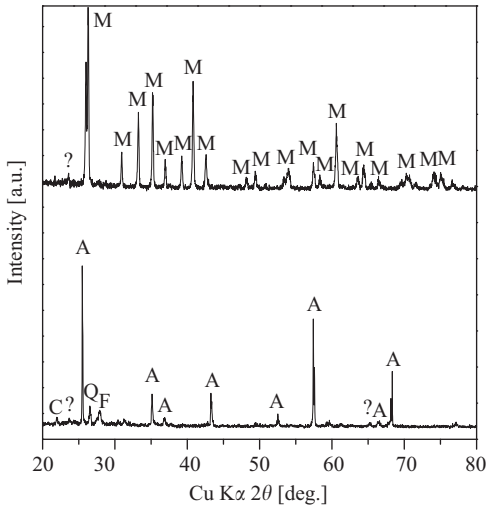

Fig. 1. XRD patterns of LC10 and CB72 samples. Symbols: *M*=mullite ($3Al_2O_3 \cdot 2SiO_2$); *A*=α-alumina (Al_2O_3); *C*=cristobalite (SiO_2); *Q*=quartz (SiO_2); *F*=feldspar ($CaO \cdot Al_2O_3 \cdot 2SiO_2$); ?=unknown.

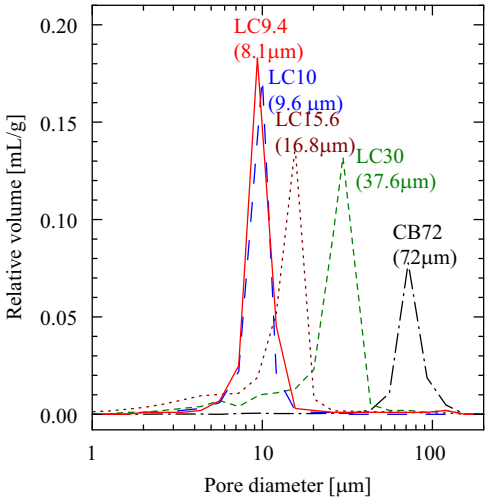

Fig. 2. Pore size distributions for the LC9.4 (continuous line), LC10 (long dashed line), LC15.6 (dotted line), LC30(short dashed line) and CB72 (dashes and dots line). The values in parentheses show the fiber diameters (μm) used as the pore formers.

The SEM micrographs of the four lotus ceramics are shown in Fig. 3. As shown in the perpendicular section (Fig. 3(a)) of LC9.4, the sizes of the single pores are less than 10 μm, but some of them are agglomerated into larger openings (up to 50 μm). The parallel section (Fig. 3(b)) shows a somewhat mixed orientation of the pores, i.e. both parallel and perpendicular to the extrusion direction. This leads to the formation of a network of three-dimensionally interconnected channels. Similar results were observed in LC10 (Fig. 3(c) and (d)). LC10 contains slightly larger single pores but fewer in number than in sample LC9.4. By increasing the diameter of the pore former, good agreement was obtained between the pore sizes seen in the SEM micrographs and the Hg-porosimetry results. Fig. 3(e) shows the pore sizes of LC15.6 to be 15–20 μm while those of LC30 (Fig. 3(g)) are about 30 μm. The SEM micrograph (Fig. 3(h)) indicates a higher degree of pore orientation arising from better orientation of the rayon fibers parallel to the extrusion direction.

The porous properties of the LC and CB samples are shown in Table 1. The bulk densities of the LC samples are very similar (1.54–1.63 g/cm^3) and their porosities range from 45.7% to 48.2%. The bulk density of CB72 is much higher (2.4 g/cm^3) than those of the LC samples due to the higher true density of α-alumina (4.0 g/cm^3) compared with mullite (3.17 g/cm^3) and also to differences in the porosities. It is expected that these differences will influence the properties for the generation of bubbles.

The gas permeability was determined from the Darcy equation [4]:

$$\mu = \frac{\eta \Delta x Q}{\Delta P A},$$

where μ is the permeability (m^2), η is the dynamic viscosity of the liquid, Δx is the thickness of the sample, Q is the flow rate, ΔP is the pressure drop between the entry point

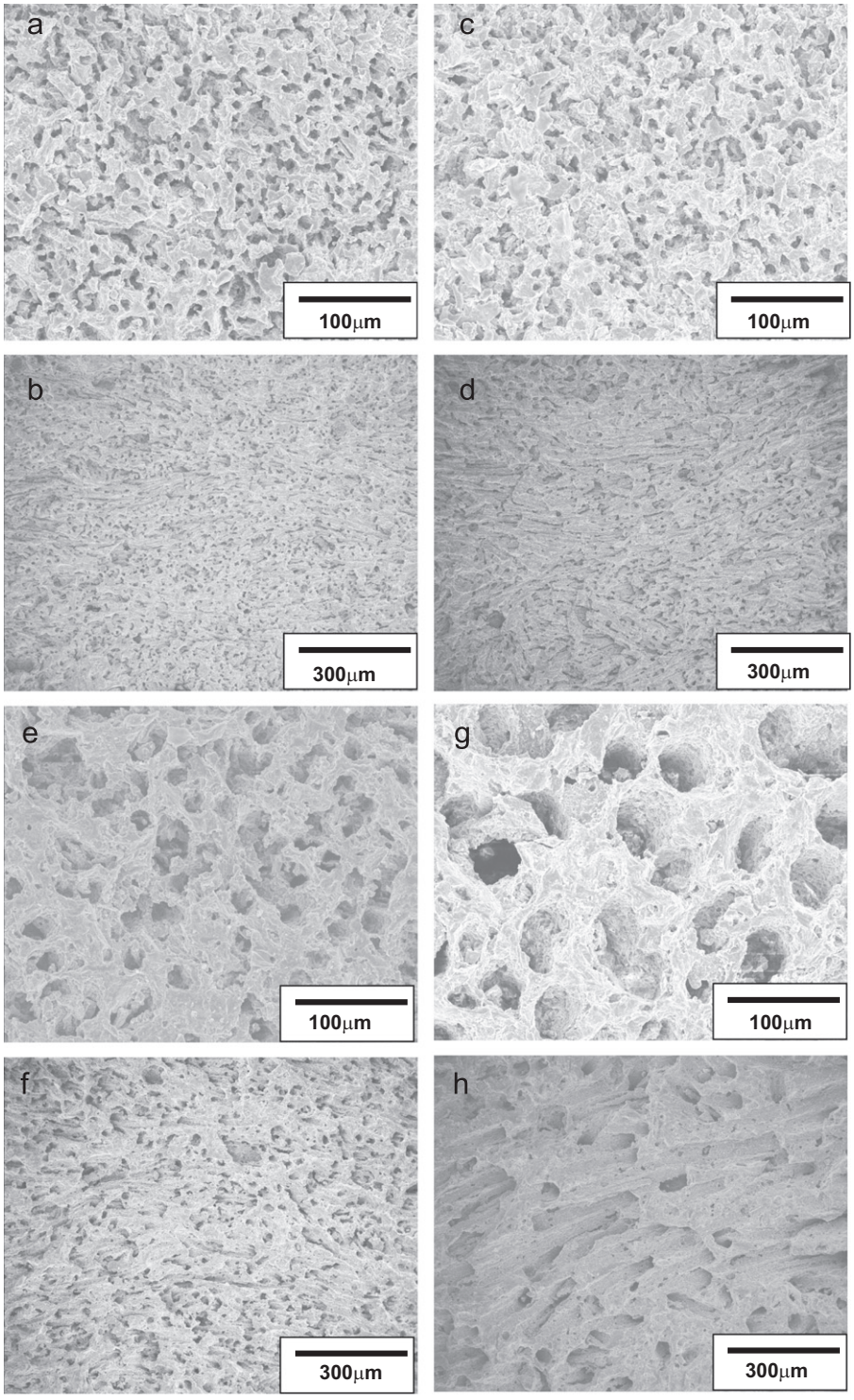

Fig. 3. SEM micrographs of the perpendicular (a) and parallel (b) sections for LC9.4, perpendicular (c) and parallel (d) sections for LC10, perpendicular (e) and parallel (f) sections for LC15.6, and perpendicular (g) and parallel (h) sections for LC30.

and exit point in the sample and A is the cross-sectional area of the sample. The gas permeability values for CO_2 and N_2 are shown in Fig. 4 as a function of pore size. The permeability (μ) of an ideal capillary system containing completely unidirectionally aligned uniformly sized cylindrical pores can be calculated from the porosity (V_P) and pore size (d) using the following equation [3]:

$$\mu = \frac{V_P d^2}{32}$$

The calculated result is shown in Fig. 4 for LC bubblers (solid line) and the CB72 bubbler (dashed line). Both CO_2

Table 1
Porous properties of the lotus ceramics and commercial bubbler.

Property	LC9.4	LC10	LC15.6	LC30	CB72
Pore size [μm]	9.4	10.0	15.6	30.0	72.0
Bulk density [g/cm^3]	1.56(4)[a]	1.63(2)	1.58(1)	1.54(1)	2.40(1)
Apparent porosity [%]	48.0(11)[a]	45.7(4)	46.5(2)	48.2(3)	28.03(1)
Bending strength [MPa]	14.0	25.5	22.0	23.0	N/A

[a]The numbers in the parentheses represent the standard deviation at the last decimal places.

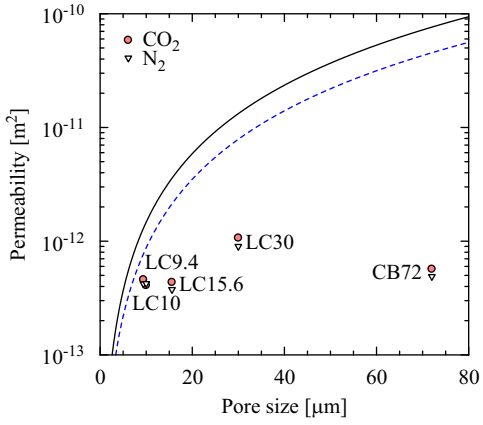

Fig. 4. Relationship between permeability of LCs and CB72 for CO_2 (solid circles) and N_2 (open reverse triangles) and pore size. The two curves represent calculated permeability of ideal capillary models for LCs (solid line) and CB72 (dashed line) using the Darcy equation.

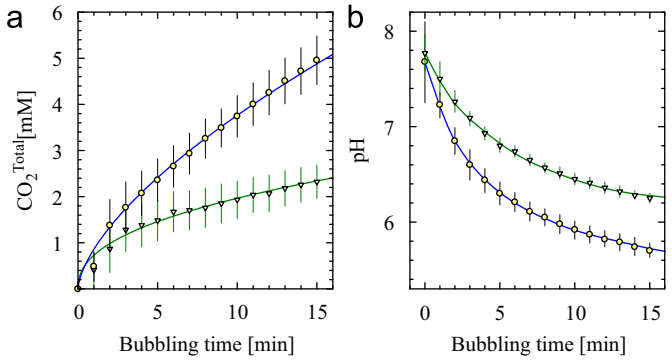

Fig. 5. Changes of CO_2 concentration (a) and pH (b) by CO_2 bubbling through LC9.4 (circles) and T3500 (reverse triangles) bubblers as a function of bubbling time. The error bars represent the standard deviation for each datum.

and N_2 gas permeability of the LC bubblers increases with increasing pore size while that of the CB72 bubbler clearly deviates from this trend, due in part to the lower porosity of CB72. However, the difference between the observed and calculated permeability data is much larger in the CB72 bubbler (μ_{Obs}/m_{Calc}=0.011) than for the LC bubblers (μ_{Obs}/m_{Calc}=0.069–0.346). This difference might arise from the difference in the microstructures of the LCs (with unidirectionally aligned pores) and CB72 (with conventional random pores). In view of their high porosity, high permeability and small pore sizes, LCs are expected to be suitable for generating small bubbles suitable for applications in CO_2 sequestration.

3.2. The effect of the pore size on the generated bubble size

To test the dissolution ability of the CO_2 bubbles in tap water, the CO_2 concentration was measured during bubbling experiments using various bubblers at a flow rate of 0.5 L/min. Typical changes of CO_2 concentration and pH for LC9.4 and T3500 bubblers are shown in Fig. 5(a) and (b) as a function of bubbling time. Both bubblers showed similar trends of convex-shaped CO_2 concentration curves and concave-shaped pH change curves. Since Back et al. [15] reported a decrease of CO_2 dissolution rate with a decrease of pH from alkaline to neutral, the decrease in the dissolution rate shown in Fig. 5(a) is similarly explained.

Table 2
Curve fitting parameters for CO_2 bubbling in tap water.

Sample	Pore size [μm]	a[a]	b[a]	R^2
LC9.4	9.4	0.861	0.641	0.9992
LC10	10.0	0.912	0.596	0.9920
LC15.6	15.6	0.827	0.621	0.9956
LC30	30.0	0.748	0.653	0.9969
CB72	72.0	0.594	0.712	0.9972
T1000	1000	0.632	0.469	0.9864
T3500	3500	0.730	0.430	0.9834

[a]CO_2 concentration = a(Bubbling time)^b

This was confirmed by the bubbling experiment at a constant pH of 3 using the LC15.6 bubbler, which showed a constant dissolution rate. The two sets of CO_2 concentration data in Fig. 5(a) were fitted using a relation of the form $y=ax^b$. The calculated results for all the samples are listed in Table 2. The order of reaction (b value) with respect to the concentration of CO_2 is in the range of 0.6–0.7 for the four LC and CB72 bubblers, but is 0.4–0.5 for the T1000 and T3500 bubblers. Thus, there is clear difference in the dissolution rates of LC9.4 and T3500. After 15 min of bubbling, the CO_2 concentrations in LC9.4 and T3500 were 5.0 mM and 2.3 mM respectively, namely twice as high a CO_2 concentration in LC 9.4. Since the difference in pore size between LC9.4 and T3500 bubblers (Table 2) is about three orders of magnitude, it is expected

that the size of the bubbles generated by the LC9.4 bubbler should be much smaller than for the T3500 bubbler which generated millimeter-sized bubbles (millibubbles).

The solubility of CO_2 in tap water is high and bubbling causes rapid dissolution, as shown in Fig. 5(a). This means that the size of the bubbles generated in tap water changes rapidly, making it difficult to observe their original size. By contrast, the solubility of air in water is negligibly small; thus, the generated air bubbles do not change their size due to dissolution. Therefore, generated bubble sizes were measured for both air and CO_2 bubbles. The cumulative volume frequencies of the generated air and CO_2 bubbles are plotted as a function of bubble size in Fig. 6(a) and (b), respectively. The air bubble size distributions for the different bubblers (Fig. 6(a)) show a clear difference, the average air bubble sizes being 455–550 μm for the LCs, 1730 μm for CB72 and 8270–8960 μm for the *T* bubblers. The order of the average air bubble sizes is in good agreement with their pore sizes. The CO_2 bubble size distributions (Fig. 6(b)) follow the same trends. The average CO_2 bubble sizes are 270–320 μm for the LCs, 1180 μm for CB72 and 7760–8820 μm for the *T* bubblers, with a similar trend being observed between the average air bubble size and the pore size. Thus, the CO_2 bubbles are found to be smaller in size than the air bubbles, reflecting the difference in the solubility of air and CO_2 in water, even though factors such as surface tension [16,17] might suggest the bubble sizes should be similar.

3.3. Evaluation of dissolved ratio of CO_2 in water

Since the dissolved ratio of CO_2 bubbled into water is very important for CO_2 sequestration applications, it was evaluated using two different methods, i.e. measurement of the CO_2 concentration in water and from the difference of air and CO_2 bubble sizes.

The following equation was used to calculate the percent of dissolved CO_2 from CO_2 concentration after bubbling for 15 min:

$$\text{Dissolved } CO_2[\%] = \frac{n_d}{n_i}100 = C_d V/(Ft(P/P_0)^{0.5}(T_0/T)^{0.5})/V_0),$$

where n_d, n_i, C_d, V, F, t, V_0, P, P_0, T, and T_0 are the amount of dissolved CO_2 (mmol), the amount of CO_2 introduced into the system (mmol), the concentration of dissolved CO_2 (mM) after bubbling for 15 min, the volume of tap water (*L*), the flow rate (L/min), the bubbling time (min), the volume (*L*) occupied by one mole of CO_2 (L/mol), the pressure measured by the pressure gauge (Pa), the atmospheric pressure (Pa), the experimental temperature (*K*) and the standard temperature (*K*), respectively. The dissolved CO_2 [%] values calculated for all the bubblers are shown in Fig. 7. The highest CO_2 dissolution ability was achieved by the LC bubbler, followed by CB72, with the lowest value being recorded for the *T* bubblers. The results clearly show an increase in CO_2 dissolution efficiency with decreasing pore size of the bubblers.

The dissolution ratio of CO_2 bubbles was also evaluated from the difference of average bubble sizes between air and CO_2 by the following equation:

$$\text{Dissolved } CO_2\ [\%] = 100\frac{4\pi r_{air}^3/3 - 4\pi r_{CO_2}^3/3}{4\pi r_{air}^3/3},$$

where r_{air} and r_{CO_2} are the average bubble sizes of air and CO_2, respectively. The calculated results are shown in Fig. 7 as a function of the pore size of the bubblers. The resulting data show an almost linear trend to higher CO_2 dissolution efficiency with smaller pore size of the bubblers. Thus, the CO_2 dissolution efficiency of the LC bubblers (75–85%) is higher than the CB72 bubbler (65–70%) and much higher than the T1000 and T3500 bubblers (5–40%). It is concluded that CO_2 bubbling by lotus

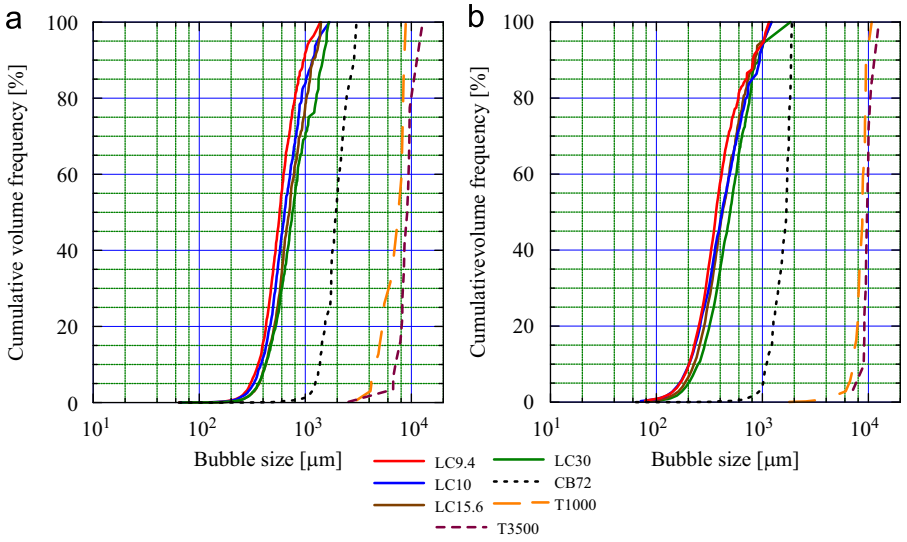

Fig. 6. Cumulative volume frequencies of the generated air (a) and CO_2 (b) bubbles through the various bubblers.

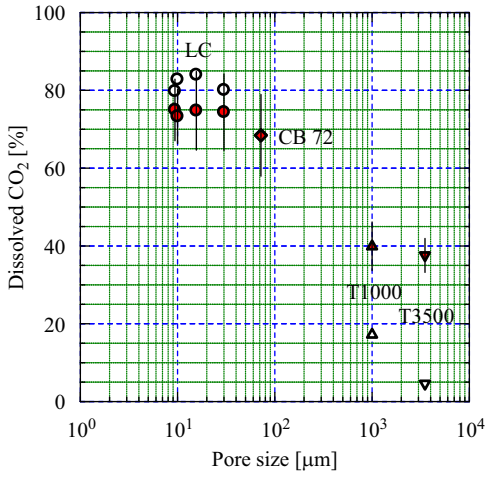

Fig. 7. Changes of dissolved CO_2 [%] in water for bubbles generated through the various bubblers as a function of pore size of bubblers. The solid symbols represent the data calculated from CO_2 concentration after bubbling for 15 min and open symbols calculated from difference in average bubble sizes of air and CO_2. The data for CB72 are overlapped.

ceramics is very effective for dissolving CO_2 gas into water without the need for special additional equipment.

4. Conclusions

This work reports the preparation of four lotus ceramics using rayon fiber pore formers of various diameters, and their characterization for an application as CO_2 micro-bubblers. The unidirectional orientation of the cylindrical pores along the extrusion direction was found to increase with increasing fiber diameter from 8.1 to 37.6 μm. Higher apparent porosity and lower bulk density was observed for the four LCs compared to a commercial bubbler CB72. Moreover, the permeability for gaseous CO_2 and N_2 increased with increasing pore size from 3×10^{-13} to 8×10^{-13} m^2 for the LCs. The pore sizes also played a significant role in the generation of smaller bubbles, since smaller pore sizes result in decreased bubble sizes. Although the LC bubblers were less than half the length of the CB72 bubbler, their unique microstructure, combined with their smaller pore sizes and higher gas permeability, led to the highest CO_2 dissolution efficiency (75–85%) without the need for any special equipment that would consume more energy.

Acknowledgments

Catalin Popa thanks the Ministry of Education, Culture, Sports, Science and Technology (MEXT, Japan) for the award of a graduate fellowship (Monbukagakusho Scholarship) under which the present study was carried out. The authors thank Professor K.J.D. MacKenzie of Victoria University of Wellington for critical reading and editing of the manuscript.

References

[1] T. Tomita, S. Kawasaki, K. Okada, A. Novel, Preparation method for foamed silica ceramics by sol–gel reaction and mechanical foaming, Journal of Porous Materials 11 (2004) 107–115.
[2] K. Okada, T. Isobe, K. Katsumata, Y. Kameshima, A. Nakajima, K.J.D. MacKenzie, Porous ceramics mimicking nature—preparation and properties of microstructures with unidirectionally oriented pores, Science and Technology of Advanced Materials 12 (2011) 064701.
[3] T. Isobe, Y. Kameshima, A. Nakajima, K. Okada, Preparation and properties of porous alumina ceramics with uni-directionally oriented pores by extrusion method using a plastic substance as a pore former, Journal of the European Ceramic Society 27 (2007) 61–66.
[4] K. Okada, S. Uchiyama, T. Isobe, Y. Kameshima, A. Nakajima, T. Kurata, Capillary rise properties of porous mullite ceramics prepared by an extrusion method using organic fibers as the pore former, Journal of the European Ceramic Society 29 (2009) 2491–2497.
[5] B.T. Lee, I.C. Kang, S.H. Cho, H.Y. Song, Fabrication of a continuously oriented porous Al_2O_3 body and its In Vitro study, Journal of the American Ceramic Society 88 (2005) 2262–2266.
[6] J. Park II, Z. Nie, A. Kumachev, E. Kumacheva, A microfluidic route to small CO_2 microbubbles with narrow size distribution, Soft Matter 6 (2010) 630–634.
[7] M. Kukizaki, Microbubble formation using asymmetric Shirasu porous glass (SPG) membranes and porous ceramic membranes—A comparative study, Colloids and Surfaces A: Physicochemical and Engineering Aspects 340 (2009) 20–32.
[8] G. Wu, Y. Wang, S. Zhu, J. Wang, Preparation of ultrafine calcium carbonate particles with micropore dispersion method, Powder Technology 172 (2007) 82–88.
[9] S. Fujikawa, R. Zhang, S. Hayama, G. Peng, The control of micro-air-bubble generation by a rotational porous plate, International Journal of Multiphase Flow 29 (2003) 1221–1236.
[10] M. Shirota, T. Imamura, M. Kameda, Formation of single bubbles from a submerged orifice using pulsed ultrasound wave, Transactions of the Japan Society of Mechanical Engineers B 72 (2006) 1220–1227.
[11] K. Okada, M. Shimizu, T. Isobe, Y. Kameshima, M. Sakai, A. Nakajima, T. Kurata, Characteristics of microbubbles generated by porous mullite ceramics prepared by an extrusion method, Journal of the European Ceramic Society 30 (2010) 1245–1251.
[12] H.N. Oguz, A. Prosperetti, Dynamics of bubble-growth and detachment from a needle, Journal of Fluid Mechanics 257 (1993) 111–145.
[13] C. Brannon Andersen, Understanding carbonate equilibria by measuring alkalinity in experimental and natural systems, Journal of Geoscience Education 50 (2002) 389–403.
[14] M.D. Abramoff, P.J. Magalhaes, S.J. Ram, Image Processing with ImageJ, Biophotonics International 11 (2004) 36–42.
[15] M. Back, M. Bauer, H. Stanjek, S. Peiffer, Sequestration of CO_2 after reaction with alkaline earth metal oxides CaO and MgO, Applied Geochemistry 26 (2011) 1097–1107.
[16] R. Massoudi, A.D. King, Effect of pressure on the surface tension of water. Adsorption of low molecular weight gases on water at 25 °C, Journal of Physical Chemistry 78 (1974) 2262–2266.
[17] W. Yan, G.-Y. Zhao, G.-J. Chen, T.-M. Guo, Interfacial tension of (methane+nitrogen)+water and (carbon dioxide+nitrogen)+water systems, Journal of Chemical and Engineering Data 46 (2001) 1544–1548.